Molecular Control of Crack Tip Plasticity Mechanisms at a PP−EPDM/PA6 Interface

Frédérique Kalb and Liliane Léger*

Laboratoire de Physique des Fluides Organisés, URA CNRS 792, Collège de France, 11 Place Marcelin-Berthelot, 75231 Paris Cédex 05, France

Costantino Creton*

Laboratoire de Physico-Chimie Structurale et Macromoléculaire, ESPCI, 10 Rue Vauquelin, 75231 Paris Cédex 05, France

Christopher J. G. Plummer

Laboratoire de Polymères, Ecole Polytechnique Fédérale de Lausanne, 1015 Ecublens, Switzerland

Philippe Marcus

Laboratoire de physique des surfaces, Ecole Supérieure Nationale de Chimie Paris, 13 rue P. et M. Curie, 75231 Paris Cédex 05, France

Arminda Magalhaes

DSM Research, P.O. Box 18, 6160 MD Geleen, The Netherlands

Received July 26, 2000; Revised Manuscript Received January 3, 2001

ABSTRACT: Adhesion between polyamide 6 (PA6) and thermoplastic vulcanizates in which the continuous phase is polypropylene (PP) have been investigated through double beam cantilever tests. Both a precise control, on molecular scales, of the surface density of bloc copolymer molecules acting as adhesion promoters and systematic observation (for scales ranging from nano- to micrometric) of the plastic deformation zones developing at the crack tip are used to identify the adhesion mechanisms. As long as the plastic deformation zones remain localized Dugdale type zones, the adhesive strength is driven by the surface density of the copolymer molecules at the interface and quantitatively follows the Brown model, whatever the detailed architecture of the crack tip deformation zone.

Introduction

The adhesion between two different materials is usually evaluated from the global mechanical stress or mechanical energy necessary to provoke failure of their common interface. More generally, however, one seeks to understand the relationship between the local molecular structure responsible for stress transfer across the interface and the energy dissipation per unit area during fracture of an adhesive joint.

When the two materials are glassy polymers, the correlation between interfacial structure and the fracture toughness, G_c, is now relatively well-known[1,2] and may be summarized as follows. If the maximum stress that can be sustained by the interface is lower than the crazing stress of both polymers, the interface fails by brittle fracture and G_c is low. If the stress that the interface can sustain is higher than the crazing stress of one of the two polymers in contact, plastic deformation mechanisms are activated on the corresponding side of the interface and an asymmetric craze propagates ahead of the crack tip. This is shown schematically in Figure 1.

In the limiting case of a relatively wide craze, the maximum width of this craze is controlled by the fibril failure stress, σ_{fibril}, and G_c is given by

$$G_c = \delta^* \frac{\sigma_{fibril}^2}{\sigma_d} \quad (1)$$

where δ^* is a parameter which depends only on the internal structure of the craze (extension ratio, fibril spacing, and longitudinal and shear moduli) and has the physical meaning of the minimum opening displacement at the crack tip ahead of which a stable craze can propagate,[3] and σ_d is the drawing stress of the polymer in the craze.

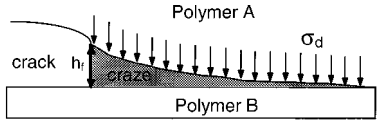

Figure 1. Schematic of a half-craze at the interface between two immiscible polymers. In this example, polymer A has a lower crazing stress than polymer B.

For the specific case in which the fibril failure stress is controlled by scission of the connecting chains (block copolymer molecules, for example) that mechanically couple the material on either side of the interface, one can also write

$$\sigma_{fibril} = \Sigma f_b \quad (2)$$

where f_b is the force to break a skeletal bond and Σ is the surface density of connecting chains at the interface. Combining eqs 1 and 2 gives the familiar prediction of Brown's model for the toughness of glassy polymers,[4] $G_c \propto \Sigma^2$. This prediction has been verified for several experimental systems involving glassy polymers.[5−7]

For semicrystalline polymers, the situation appears more complicated since the morphology and degree of crystallinity near the interface depend on the details of the processing conditions. They are likely to influence both the mechanical coupling between the connecting

* To whom correspondence should be addressed

10.1021/ma001318e CCC: $20.00
Published on Web 03/16/2001

chains and the material on either side of the interface and the local plastic deformation mechanisms.

For joints between isotactic polypropylene and polyamide-6 (PP/PA6), Boucher et al.[8] have shown the fracture toughness of the interface to be directly proportional to the square of the surface density of block copolymer molecules present at the interface, i.e., $G_c \propto \Sigma^2$, as for glassy polymers. (The copolymer molecules were formed in situ during annealing of the assembly by reaction of polypropylene-*g*-maleic anhydride (PP-*g*-MAH) chains present in the PP with the amine terminal groups of the PA6.) This result was obtained for PP-*g*-MAH chains of two different lengths and demonstrates unequivocally that the important parameter for the adhesive strength in this case is neither the annealing temperature nor the annealing time, but Σ.

In a subsequent study, it was shown that with the longer grafted PP-*g*-MAH chains, the fracture toughness could be further enhanced by a factor of 4 for annealing temperatures larger than 223 °C.[9] Electron microscopy observations of these tougher interfaces[10] demonstrated that, under such annealing conditions, extensive diffuse deformation was present beyond the main plastic zone and G_c was no longer related to the interfacial structure by eq 1.

In the work presented here, we have investigated an experimental system similar to PP/PA6 in its interfacial structure but very different in its bulk properties. The PP side of the interface is a blend of PP and ethylene-propylene-diene monomer (EPDM) elastomer where the majority phase is EPDM, but the continuous phase is PP. This type of material is of great industrial interest since it has mechanical properties close to those of an elastomer, but can be processed by standard injection molding and extrusion techniques. We shall refer to this blend as a thermoplastic vulcanizate (TPV).

As in the system investigated by Boucher et al., the interface was reinforced with PP−PA6 diblock copolymer molecules. These were again formed in situ during annealing of the assembly by reacting PP-*g*-MA chains dissolved in the PP phase of the TPV with the PA6 terminal amine groups. Σ and G_c were measured using, respectively, X-ray photoelectron spectroscopy (XPS) and an asymmetric double cantilever beam test. In combination with microscopic observations of the deformation mechanisms in the plastic zone at different length scales, this has allowed us to establish a comprehensive picture of the correlation between the interfacial structure at the molecular level and the adhesive toughness, G_c, in this system.

Experimental Section

Materials. The PA6 was Ultramid B-3 from BASF. Two model TPVs were prepared from of a blend of PP, EPDM and a phenolic resin that acted as a cross-linking agent (see Table 1). The blends were extruded by DSM Research to give phase-separated structures with a continuous PP matrix and a cross-linked EPDM dispersed phase. The molecular characteristics of all the base polymers are given in Table 2 and the compositions of the two TPVs are given in Table 3.

PP-*g*-MA chains, provided by Elf-Atochem, were incorporated into the TPV using a mini-mix extruder (capacity 5 g). Three different blends were prepared: TPV70 + 3.3 wt % PP-*g*-MA, TPV70 + 15.3 wt % PP-*g*-MA, and TPV55 + 15.3 wt % PP-*g*-MA. The percentages are given relative to the weight of PP matrix. To permit quantitative interpretation of the fracture tests, the elastic moduli and yield stresses of the beams needed to be determined at the test temperature and at an appropriate deformation rate. This was done using a three-point bending test, and the results are compiled in Table 4.

Table 1

% ethylene	% propylene	% 2-ethylidene norbornene
67	28.5	4.5

Table 2

	M_w (kg/mol)	M_N (kg/mol)	av MA/chain
PA6	25	13	
PP matrix	520	77	
PP-*g*-MA	142	43	0.86

Table 3

	% PP	% EPDM	% phenolic resin
TPV55	46	52	0.8
TPV70	29	68	1.1

Table 4

	elastic modulus (E)	yield stress (σ_y), MPa
PA6	2.2 GPa	65
matrix PP	1.25 GPa	27
TPV55	125 MPa	7
TPV70	55 MPa	4

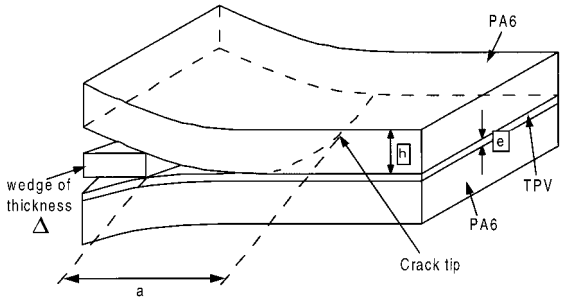

Figure 2. Geometry of the sandwich DCB test.

The PA6 was then molded into 2 mm thick plates and the TPV + PP-*g*-MA blends pressed into 400 μm thick films. Prior to annealing, the PA6 and TPV specimens were thoroughly washed in ethanol, dried under nitrogen, and further dried at 80 °C under vacuum in order to minimize the effect of moisture on the mechanical properties of the PA6 and to establish a rigorous experimental protocol.

Mechanical Tests. Since the different TPVs were much softer than the PA6 (their elastic moduli were on the order of 50−100 MPa), it was necessary to adapt the simple asymmetric double cantilever beam (DCB) geometry widely used to test interfaces between hard polymers. Fracture tests were therefore carried out on specimens machined from plaques prepared by placing a TPV film between two PA6 plates. The resulting PA6/TPV/PA6 sandwiches were then annealed at temperatures between 185 and 225 °C for 100 to 800 min in a closed mold. After annealing, they were cooled slowly to room temperature in the mold at a rate of 4 K/min.

The sandwich DCB test geometry is shown in Figure 2. The deformation of the beams was dominated by the elastic response of the PA6, making the calculation of G relatively straightforward. However, the resistance to crack propagation, G_c, was that of the interface between the TPV and the PA6. To take into account the presence of the soft TPV layer, the beam on an elastic foundation model[11] for the DCB test was modified. The details of the calculation, based on earlier work by Penado,[12] are given in Appendix I. G_c was evaluated from the following expressions:

$$G_c = \frac{3}{8}\frac{\Delta^2}{a^4}\frac{E_{PA}h_1^3 E_{eq}(h_2+e)^3}{E_{PA}h_1^3\alpha_2^2 + E_{eq}(h_2+e)^3\alpha_1^2} \qquad (3)$$

with

$$\alpha_i = \left(\frac{1 + 3/\lambda_i a + 3/\lambda_i^2 a^2 + 3/2\lambda_i^3 a^3}{1 + 1/\lambda_i a}\right)$$

and

$$\lambda_i = \left(\frac{h_i^4}{6} + \frac{E_{PA} h_i^3 e}{8 E_{TPV}}\right)^{-1/4}$$

where Δ, a, h_1, h_2, and e are defined in Figure 2, E_{TPV} and E_{PA} are respectively the elastic moduli of the TPV and the polyamide, and E_{eq} is the equivalent bending modulus of the PA + TPV compound beam of thickness $h_2 + e$.

The test was performed on an Adamel Lhomargy DY32B tensile test machine, and the wedge was a razor blade pushed along the interface at a constant speed of 0.2 mm/min (3.3 μm/s). Although measurements were made during crack propagation, in what follows we shall only discuss values obtained after full relaxation of the crack length.

XPS Characterization of the Copolymer Layer Formed at the Interface. The technique developed by Boucher et al. was used to determine the surface density of PA6−PP diblock copolymer molecules formed at the interface.[8] An unbroken part of the sandwich specimen was immersed in a formic acid bath in order to dissolve the two PA6 beams. Four successive formic acid baths and vigorous stirring were necessary to fully dissolve the PA6. The PA6 chains that had reacted with the PP-*g*-MA during the annealing step of the joint were not dissolved away by the formic acid and formed, after drying, a thin PA6 layer at the surface of the TPV film. The treatment with trifluoroacetic anhydride recommended by Boucher et al. was found to be unnecessary with adequate stirring.

Since the grafted PA6 chains contained nitrogen, given suitable control specimens (pure PA6 and pure PP) and a reasonable model for the organization of the layer, their surface density could be quantified by XPS. The XPS experiments were carried out using the magnesium K_α line of the VG ESCALAB Mk II spectrometer (energy 1253.6 eV, natural width 0.7 eV). The analyzed area was approximately 2 mm × 5 mm and the detection angle was normal relative to the surface. To avoid degradation of the layer, the incident power was limited to 200 W. The 1s spectra of carbon, nitrogen, and oxygen were analyzed in that order, and a final complete spectrum was then taken to check for the presence of contaminants. This measurement protocol was strictly adhered to because of the risk of degradation of the layer.

Only the C 1s and N 1s spectra were used in the analysis and the relative intensity of the two peaks compared. Modeling was based on the assumption of the presence of a dense layer of PA6 of variable thickness at the surface, as detailed previously.[8] The grafted PA6 chains at the interface were assumed to have a molecular weight distribution representative of that of the bulk PA6 (a reasonable assumption since all PA6 chains have one reactive group and since no long-range diffusion is necessary for the PA6 to react at the interface). The surface density of copolymer chains at the interface was then calculated from

$$\Sigma = -\left(\frac{N_a \rho}{M_n}\right)\lambda(\sin\theta)\ln\left(1 - \frac{I_N/I_C}{(I_N^\infty/I_C^\infty)^{PA}}\right) \qquad (4)$$

where λ is the mean free path of the photoelectrons, I_N^∞ and I_C^∞ are the intensities of the carbon and nitrogen peaks on the pure PA6 surface, N_a is Avogadro's number, ρ is the density of the polymer and M_n is the number-average molar mass of the PA6 chains.

Observation of Local Plasticity Processes. Certain fracture specimens were embedded under stress (i.e., with the wedge in place) in either a commercial epoxy resin (Araldite D and hardener HY956 from Ciba) or in methyl methacrylate (MMA) in order to preserve as far as possible the original morphology of the deformed regions. After polymerization of the resin at room temperature and an overnight heat treatment at 80 °C to further harden the resin, the block was trimmed. Thin sections were then prepared from regions around the crack tip in the plane perpendicular to the plane of the interface and about halfway through the specimen thickness. Sections for observation by transmission optical microscopy were prepared using a glass knife and were several micrometers thick. The block surface could also be observed in reflected light if necessary.

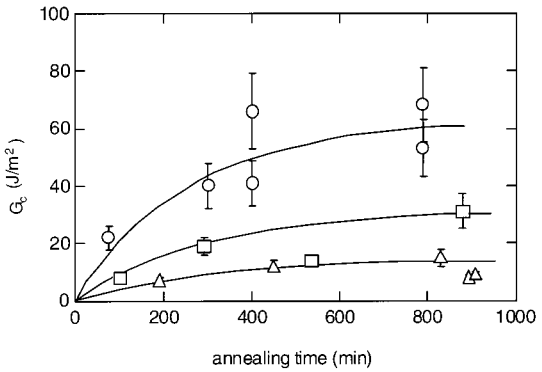

Figure 3. Fracture toughness G_c of TPV/PA6 interfaces as a function of annealing time: (○) TPV70 + 15 wt % PP-*g*-MA; (□) TPV70 + 3 wt % PP-*g*-MA; (△) TPV70.

For transmission electron microscopy (TEM), ultrathin sections (80−100 nm) were prepared using two different methods. For the microdeformations micrographs (Figures 11 and 12), the specimens were stained by overnight exposure to RuO_4 vapor prior to sectioning and re-stained and re-sectioned at least once in order to remove any surface artifacts left over from the trimming procedure. For optimum penetration of any cavities immediately ahead of the crack tip, samples embedded in PMMA were generally preferred. The microtoming was done with a Reichert-Jung Ultracut E ultramicrotome and a Diatome 35° diamond knife at room temperature. Bright field TEM micrographs were obtained using either the Philips EM 430 at 300 kV or the Philips CM20 at 200 kV depending on their availability. For the morphology micrographs (Figure 8), the thin films were microtomed at −120 °C and subsequently stained for 30 min in RuO_4 vapor. Images were obtained on a Philips CM200 microscope at 120 kV.

Results

In most of this study the annealing temperature was fixed at 200 °C, a temperature high enough to melt the PP matrix of the TPV, but low enough to permit us to follow the grafting kinetics using the present experimental protocol. Industrial applications use significantly higher annealing temperatures in order to accelerate the reaction, but it was not the aim of the present fundamental study to optimize the grafting kinetics.

Figure 3 shows G_c as a function of the annealing time for three different blends with identical mechanical properties but presumably a different interfacial structure, since the amount of PP-*g*-MA in the blends was varied. An unexpected result was the abnormally high adhesion of TPV70 to PA6 when no PP-*g*-MA was present in the blend. For comparison, bonding of PP/PA6 interfaces in the absence of PP-*g*-MA led to $G_c \approx 1$ J/m^2 (and to spontaneous delamination of the two materials). Nevertheless, when PP-*g*-MA was added to the TPV (3 wt %, or 15 wt % relative to the weight of the PP), the measured G_c increased significantly, with an even more pronounced improvement in G_c when the amount of PP-*g*-MA in the blend was increased. Similar results were also obtained at lower EPDM contents as shown in Figure 4. However, unlike the PP/PA6 interfaces, where the measured G_c reached a limiting value in the presence of PP-*g*-MA after long annealing times,

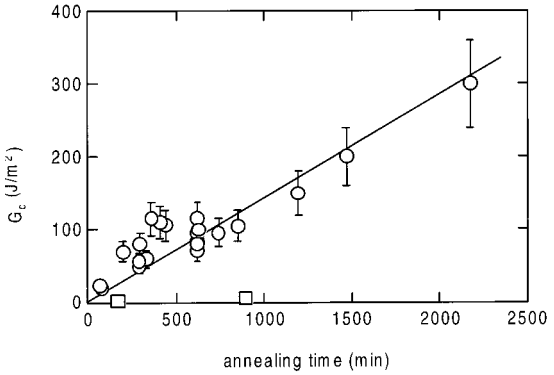

Figure 4. Fracture toughness G_c of TPV/PA6 interfaces as a function of annealing time: (○) TPV55 + 15 wt % PP-*g*-MA; (□) TPV55.

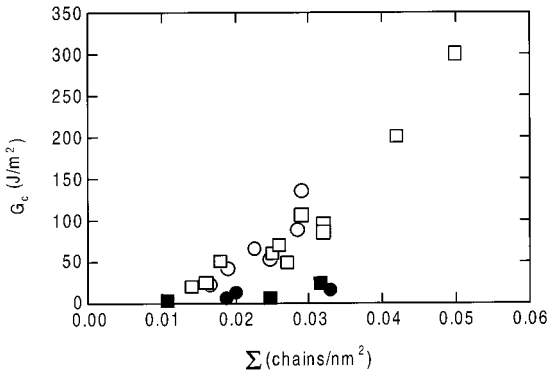

Figure 5. Fracture toughness G_c of TPV/PA6 interfaces as a function of the surface density of PA6 grafted chains at the interface, Σ: (□) TPV55 + 15 wt % PP-*g*-MA; (○) TPV70 + 15 wt % PP-*g*-MA; (■) TPV55; (●) TPV70.

depending on the annealing temperature, the TPV/PA6 interfaces showed no obvious limiting value of G_c.

The correlation between G_c and Σ, determined by XPS, is shown in Figure 5. Regardless of the amount of EPDM and PP-*g*-MA initially present in the blend, all the assemblies annealed at 200 °C gave results that fell on two master curves: one for the case where PP-*g*-MA was present and one when no PP-*g*-MA was present. The first case (with PP-*g*-MA) is consistent with the previous observations of the behavior of PP/PA6 blends referred to in the Introduction. It is more surprising, however, that a similar master curve could be obatained for TPV/PA6 joints prepared without PP-*g*-MA. This clearly indicates direct grafting between the TPV and the PA6, although this direct reaction was considerably less effective mechanically than grafting of PP-*g*-MA to the PA6.

These general trends are even more apparent in the log−log plot of Figure 6. Where PP-*g*-MA was present in the TPV, linear curve fitting suggested $G_c \propto \Sigma^{2.16\pm0.17}$, i.e., quite close to a quadratic dependence. Although fewer data were available for the unmodified TPV, there appeared to be a similar dependence of G_c on Σ, albeit with a different constant of proportionality. Possible grafting mechanisms leading to this behavior are examined in more detail in the next section.

Structure of the Interface at the Molecular and Microscopic Levels. The XPS results raise two main questions: What is the reaction mechanism responsible for the grafting reaction between the TPV and the PA6, and what is the structure of the molecular species formed at the interface?

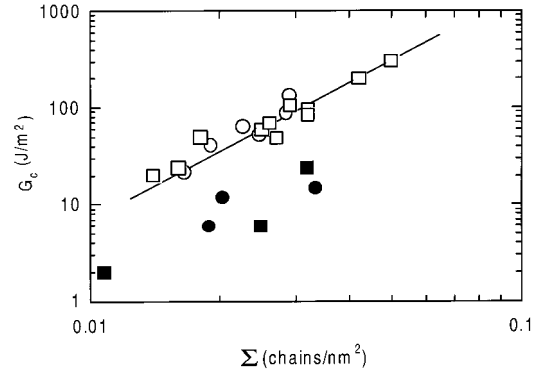

Figure 6. A log−log plot of G_c vs Σ for the TPV/PA6 interfaces: (□) TPV55 + 15 wt % PP-*g*-MA; (○) TPV70 + 15 wt % PP-*g*-MA; (■) TPV55; (●) TPV70.

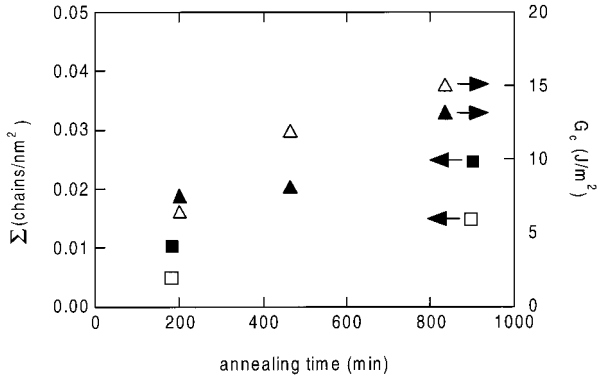

Figure 7. Σ and G_c of interfaces between PA6 and TPV with different EPDM contents as a function of annealing time: (□) Σ for TPV55; (■) Σ for TPV70; (△) G_c for TPV55; (▲) G_c for TPV70.

When the TPV contains PP-*g*-MA, both grafting mechanisms are active, i.e., the formation of PP−PA6 copolymers and the reaction of PA6 with the pure TPV. Do they compete?

We first consider the reaction between TPV and PA6. It is highly unlikely that unfunctionalized PP could react with PA6, as borne out by the observation of negligible adhesion between pure PP and PA6, even after long annealing times.[8] On the other hand, EPDM in the TPV contained about 1 wt % of a cross-linking agent intended to cross-link the EPDM dynamically during processing of the blend. This cross-linking agent was an oligomeric phenolic resin capable of decomposing to form reactive carbocations which could then react with the unsaturated bonds of the EPDM.[13] Most of these will be consumed during the cross-linking reaction, but a certain proportion of cations already associated with the EPDM rubber may be able to react with an amine or an amide group of the PA6, effectively grafting an EPDM particle to the PA6.[14,15] Experimental evidence that it was the EPDM that reacted with the PA6 is given in Figure 7. For a given annealing time, Σ and G_c were both greater for TPV70 than for TPV55. Further experimental evidence is provided by TEM observations of the interface of the annealed specimens (Figure 8). Although a significant amount of EPDM was present at the interface in a pure TPV70/PA6 assembly (Figure 8a), a depletion layer containing only PP was always visible at the interface between TPV70 + PP-*g*-MA and PA6 (Figure 8b). Presumably when the PP-*g*-MA is present in the blend, it can react relatively rapidly with the PA6, thus stabilizing the interface. In the absence of PP-*g*-MA, the TPV minimizes its inter-

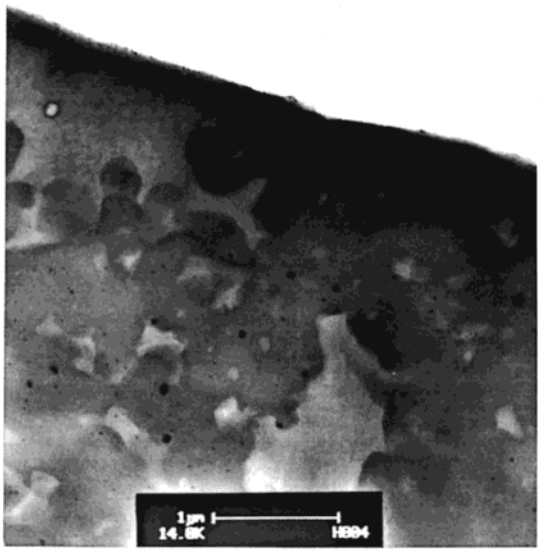

a

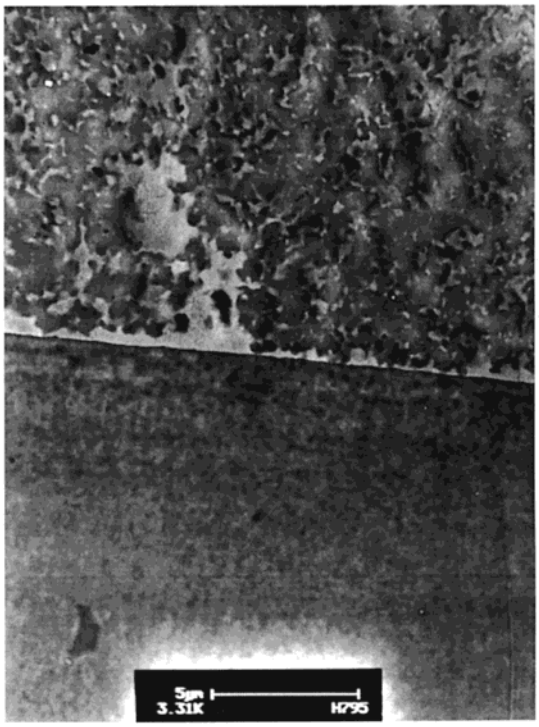

b

Figure 8. (a) TEM micrograph of the microstructure at an interface between pure TPV70 and PA6 (the PAG part has PA6). (b) TEM micrograph of the microstructure at an interface between TPV70 + 15 wt % PP-*g*-MA and PA6.

facial tension with PA6 through segregation of the more polar EPDM particles to the interface. The reaction between the EPDM and the PA6 then effectively anchors the rubber particles to the interface.

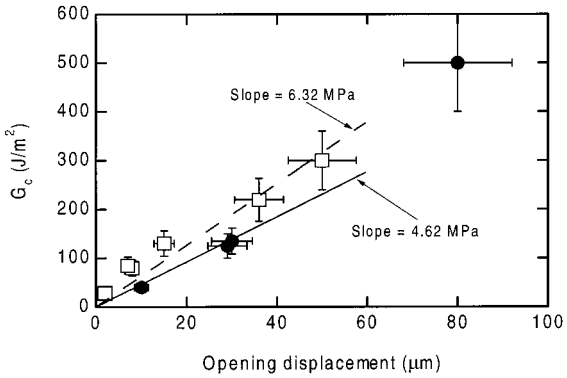

Figure 10. G_c as a function of h_f for (●) TPV55 and (□) TPV70 both with 15 wt % PP-*g*-MA against PA6.

Fracture Mechanisms of the Interface. An important aspect of any study of fracture mechanisms is the identification of the microscopic deformation mechanisms responsible for energy dissipation. In hard systems, such as glassy polymers, this dissipation is highly localized to the vicinity of the crack tip, whereas in very soft systems, such as pressure-sensitive adhesives, dissipation is diffuse and can take place over a volume on the order of the specimen size. Since the TPVs are of intermediate elastic modulus, it is particularly interesting to investigate whether the deformation is localized or diffuse and over which volume it develops.

An optical micrograph of a typical crack tip deformation zone is shown in Figure 9. It appears relatively localized, adopting the elongated wedge shape of a Dugdale plastic zone. However, it is much greater in extent than similar zones observed in glassy or hard semicrystalline polymers. This may be rationalized as follows. According to Dugdale's model, the maximum width of the plastic zone, h_f, should vary as

$$h_f = \frac{G_c}{\sigma_d(1 - 1/\lambda)} \tag{5}$$

where λ is the extension ratio in the plastic zone. Figure 10 shows G_c as a function of h_f for TPV55 and TPV70. In both cases, G_c increased linearly with h_f, and σ_d could therefore be estimated from the slopes of the curves. Taking λ to be 3, these slopes (9.48 MPa for TPV55 and 6.93 MPa for TPV70) compare relatively well with the yield stresses of the two blends in tension, as shown in Table 4.

More detailed information on the microdeformation at the crack tip in the TPV/PA6 joints could be obtained by TEM as shown in Figures 11 and 12. Figure 11 gives an overview of the microdeformation at an interface for which G_c was about 200 J/m^2, along with a schematic

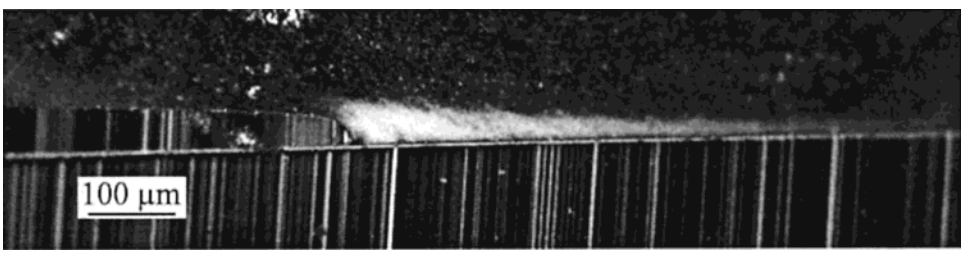

Figure 9. Optical micrograph of the crack tip deformation zone at an interface between TPV55 + 15 wt % PP-*g*-MA and PA6. G_c was 220 J/m^2 in this case.

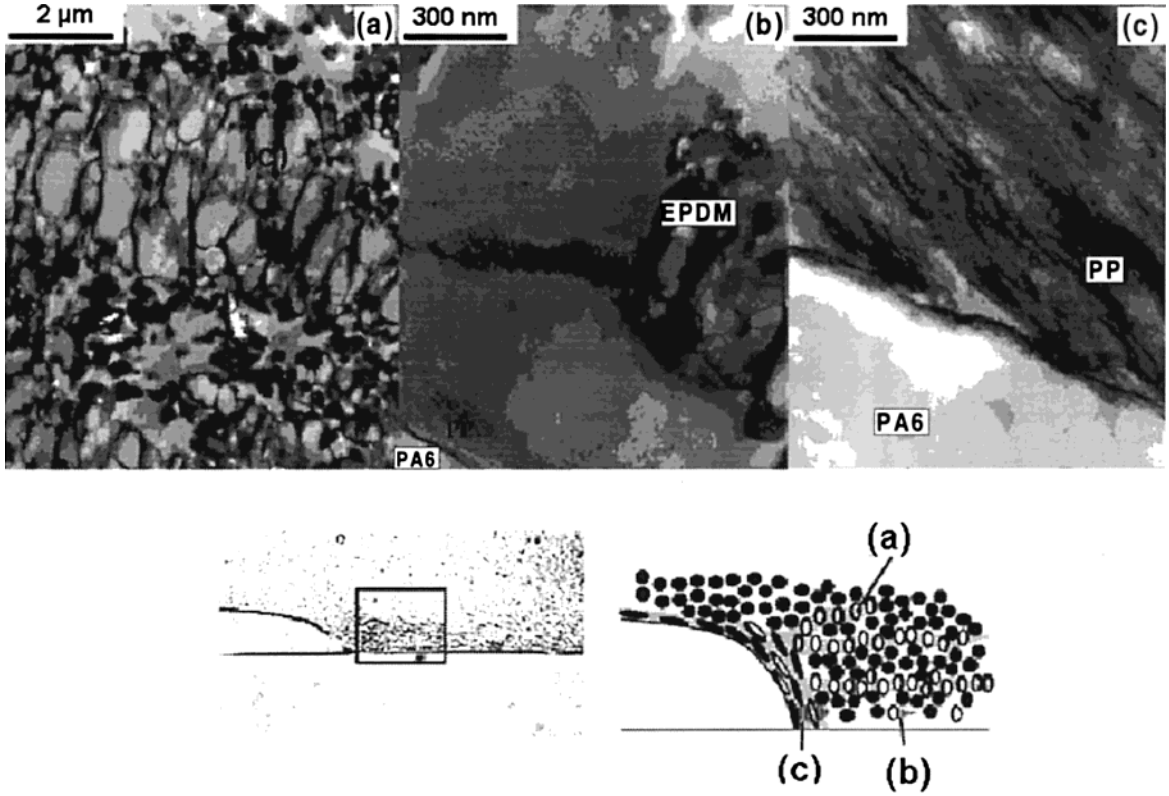

Figure 11. TEM micrographs of microdeformation from different parts of a TPV55/PA6 interface embedded in PMMA and stained with RuO_4. Also shown are an optical image of the entire deformation zone and a schematic indicating the region corresponding to each image.

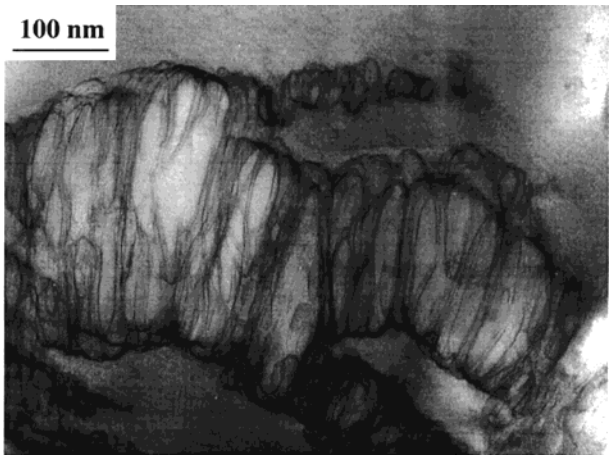

Figure 12. Detail of a craze close to the interface of the specimen in Figure 11.

of the principal mechanisms involved. Unlike the crazelike deformation zones observed ahead of crack tips at PP/PA6 interfaces[10] in the case of TPV/PA6, deformation did not appear to initiate at the interface itself. Rather, assuming the peripheral regions of the (arrested) deformation zones to represent the earliest stages in their development, cavitation of the EPDM particles preceded substantial matrix deformation.

As shown in Figure 11a, in the essentially two-dimensional thin sections, the cavitated EPDM particles were arranged in rows running roughly perpendicular to the principal stress direction. These rows of cavitated particles were primarily responsible for the texture that defined the deformation zone in the optical micrographs. They are typical of crack tip deformation in rubber-modified systems with relatively uniform particle diameters.[16] However, it is significant that since the TVP was depleted of EPDM particles in the regions immediately adjacent to the interface for the reasons discussed in the previous section, no substantial particle cavitation could be seen at the interface itself. It is also apparent from Figure 11a that continued deformation led to plastic dilatation and elongation of the cavities in the direction of the principal stress, through progressive drawing down of the intervening PP matrix ligaments. There was no evidence of crazelike deformation in regions containing relatively high particle densities. On the other hand, close to the interface and in other regions locally rich in PP, crazes were seen, as shown in Figure 11b, these tending to originate from modifier particles adjacent to the depletion layer. It was only in the regions of the deformation zone very close to the crack tip (Figure 11c**)** that deformation spread to the whole matrix, resulting in a highly inhomogeneous structure consisting of stretched cavities, particles, matrix ligaments, and crazes. This structure then failed at or very close to the interface to form the crack proper, as was apparent from the lack of debris on the crack surfaces corresponding to the PA side.

Figure 12 shows a detail from a craze in the depletion layer adjacent to the interface embedded in PMMA, showing the internal structure. Although the craze had undergone some distortion during sample preparation, fibrils were clearly distinguishable, their diameters (about 10 nm) being similar to those observed in crazes at PP/PA6 interfaces.[10]

Discussion

On the basis of the experimental results of the three preceding sections, we can now propose a general

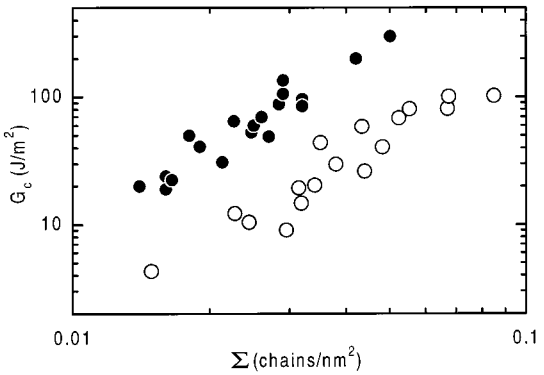

Figure 13. G_c as a function of Σ: (●) TPV/PA6 interfaces; (○) PP/PA6 interfaces.

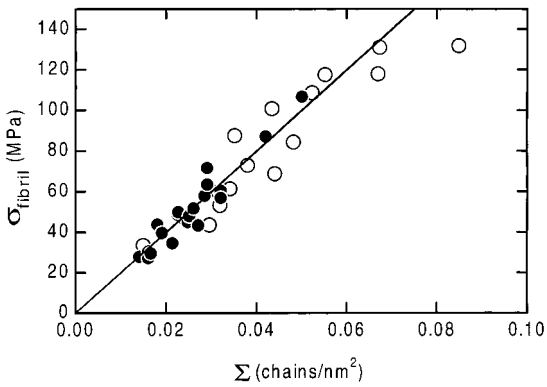

Figure 14. Estimated fibril failure stress as a function of Σ: (solid curve) $\sigma_{fibil} = \Sigma f_b$; (●) results for TPV/PA6; (○) results for PP/PA6.

picture for the adhesion mechanisms of the PP-based TPVs with PA6. Stress transfer at the interface is provided by PP−PA6 copolymers formed by the interfacial reaction of the amine terminal group of the PA6 chains with the MA group of the PP-*g*-MA dissolved in the PP matrix of the TPV. The similarity with the PP/PA6 joints is striking, as is further demonstrated by the direct comparison of the two systems shown in Figure 13. In both cases, G_c increased as Σ^2. The absolute values of G_c were nevertheless much higher for TPV/PA6 for a given Σ. This is readily explicable in terms of the different drawing stresses of PP and of TPV. Assuming the other factors in eq 1, i.e., δ^* and σ_{fibril}, not to be substantially different for the two materials, G_c is predicted to vary as σ_d^{-1}, consistent with the roughly 5-fold increase in G_c on going from PP/PA6 to TPV/PA6, and the data in Table 4. Physically, this implies that the load-bearing structure at the interface is identical in the two types of interface (borne out by the surface analysis results) and that the internal structure of the respective plastic zones is also very similar. This is somewhat surprising, given that the TEM observations indicate very different morphologies. However, at least for the range of conditions considered up to now, the plastic zones in the TPVs were localized and their overall form consistent with Dugdale's model. It may also be inferred from the TEM results that the fibrillar structure at the interface itself was very similar in TPV/PA6 and PP/PA6, at least in the immediate vicinity of the crack tip, owing to the presence of the EPDM-depleted layer at the TPV−PA6 interface.

A way of testing the above hypothesis is to calculate the fibril failure stress in each system, as shown in Figure 14. This fibril failure stress was obtained by first fitting the G_c vs Σ data for the PP−PA6 interfaces to obtain a value of δ^* using eqs 1 and 2. The fibril failure stress σ_{fibril} was then obtained from the following expression:

$$\sigma_{fibril} = \sqrt{\frac{G_c \sigma_d}{\delta^*}}$$

It is clear from Figure 14 that the fibril failure stresses calculated from Brown's model using the measured values of G_c and σ_d (where an average value of σ_d = 5 MPa was taken for the TPV systems) all lie on a single straight line. This is a remarkable result, which extends the domain of validity of the physical concept of stress transfer in the plastic zone as a failure mechanism.

What are the limits of the approach? When the annealing temperature of the assemblies was increased above 200 °C, they became extremely difficult to fracture and the measured G_c were correspondingly high. Optical observations of the plastic zone in such cases showed that deformation took place in an extensive volume of the TPV film beyond the localized Dugdale zone. The correlation between G_c and the thickness of the plastic zone was accordingly lost. Thus, use of the method of Figure 14 to calculate σ_{fibril} led to gross overestimates, showing clearly that Brown's model is no longer applicable in the presence of diffuse crack tip deformation.

Conclusion

We have shown conclusively that the adhesion between PA6 and PP−EPDM blends can be controlled by the grafting of PP-*g*-MA to the PA6 at the interface. The fracture toughness G_c increased with the square of the surface density of copolymer chains formed in situ during annealing and was directly related to the width of a localized Dugdale plastic zone at the interface. Furthermore, the G_c values for the TPV/PA6 assemblies were directly proportional to those of PP/PA6 assemblies with identical grafting densities. The proportionality constant was given by the reciprocal of the ratio of the drawing stresses of TPV and PP, in perfect agreement with Brown's model for the toughness of glassy polymers.

This remarkable result implies that the predictions of Brown's model are insensitive to the details of the architecture of the crack tip deformation zone, depending only on the existence of a localized Dugdale type zone which can transfer stress laterally and has a constant drawing stress as a boundary condition.

Appendix 1

To extract the adhesion energy from the fracture length and the mechanical properties of the two beams, Kanninen's approach had to be adapted to the sandwich geometry of Figure 2. We present here the main steps of the calculations leading to a satisfactory description of the mechanics of the DCB test in the sandwich geometry with a soft film intercalated between two hard beams. Two main adaptations have to be introduced.

The first modification is straightforward. The two beams are not mechanically symmetric. One beam is a composite one, with the soft film attached to it. The effective elastic modulus of the composite beam, E_{eq}, i.e., that of the equivalent homogeneous beam with a thick-

ness $h + e$, where h and e are, respectively, the thickness of the PA6 and of the TPV layer, has to be introduced. E_{eq} has been measured by a three-points flexion test. The elastic energy stored in the beams, for a simple embedded beam, is then given by

$$G_c = \frac{3}{8}\frac{E_{eq}(h+e)^3\Delta^2}{a^4} \tag{A1}$$

with Δ the thickness of the razor blade and a the length of the fracture.

The second modification is more delicate. The soft film allows the beams to be deformed well ahead the crack tip so that the Kanninen elastic foundation needs to be adapted to incorporate the elastic properties of the soft film. We detail below the main steps of this modification, following the general ideas introduced by Penado, but adapted to the case of our materials for which the elastic modulus are 50 times weaker than for the situation investigated by Penado.

Considering the TPV layer and the PA6 as two springs mounted in series, the elastic modulus of the elastic foundation is

$$\mathrm{k} = \frac{1}{\frac{1}{k_{PA6}} + \frac{1}{k_{TPV}}} \tag{A2}$$

with

$$k_{PA6} = 2\frac{E_{PA6}b}{h}$$

as for the simple situation without TPV (b is the width of the beam), and k_{TPV} evaluated assuming a state of plane stress in the TPV, i.e.

$$k_{TPV} = \frac{2E_{TPV}b}{e(1-\nu^2)}$$

where ν is the Poisson coefficient of the TPV, taken to be approximately 0.5. Equation A2 can thus be rewritten as

$$k = \frac{1}{\frac{h}{2E_{PA6}b} + \frac{3}{8E_{TPV}b}} \tag{A3}$$

As the elastic modulus of the PA6 is much larger than that of the TPV, equation A3 finally reduces to

$$k \approx k_{TPV} = \frac{8E_{TPV}b}{3e} \tag{A4}$$

This means that this is essentially the soft TPV layer that allows the deformation of the beams ahead the fracture tip. The Kanninen solution for the deflection of the beam is then the classical one, with

$$\lambda = \left(\frac{h^4}{6} + \frac{E_{PA6}h^3b}{8E_{TPV}b}\right)^{-1/4} \tag{A5}$$

Taking into account the fact that the two PA6 beams may not have exactly the same thickness, the stored elastic energy in each beam is then given by the Kanninen expression, written with the corresponding PA6 thickness and the corresponding λ values, i.e.

$$G_c^{PA6} = \frac{3}{8}E_{PA6}{h_1}^3\delta_1$$

$$G_c^{PA6} = \frac{3}{8}\frac{E_{PA6}{h_1}^3\delta_1}{a^4{\alpha_1}^2} \tag{A6}$$

and

$$G_c^{PA6+TPV} = \frac{3}{8}\frac{E_{eq}(h_2+e)^3{\delta_2}^2}{a^4{\alpha_2}^2} \tag{A7}$$

with

$$\alpha_i = \left(\frac{1 + 3/\lambda_i a + 3{\lambda_i}^2a^2 + {}^3/_2{\lambda_i}^3a^3}{1 + 1/\lambda_i a}\right)$$

and

$$\lambda_i = \left(\frac{{h_i}^4}{6} + \frac{E_{PA6}{h_i}^3\mathrm{e}}{8E_{TPV}}\right)^{-1/4}$$

The total adhesion energy can thus be obtained by minimizing the total elastic energy stored in the two beams, imposing the total deflection to be $\delta_1 + \delta_2 = \Delta$, the thickness of the blade. One gets

$$G_c = \frac{3}{8}\frac{\Delta^2}{a^4}\frac{E_{PA6}{h_1}^3E_{eq}(h_2+e)^3}{E_{PA6}{h_1}^3{\alpha_2}^2 + E_{eq}(h_2+e)^3{\alpha_1}^2} \tag{A8}$$

with the expressions of α_i and λ_i defined above.

References and Notes

(1) Kramer, E. J. *Plast., Rubber Compos. Process. Appl.* **1997**, *26*, 241−249.
(2) Kramer, E. J.; Norton, L. J.; Dai, C. A.; Sha, Y.; Hui, C. Y. *Faraday Discuss.* **1994**, *98*, 31−46.
(3) Creton, C.; Kramer, E. J.; Brown, H. R.; Hui, C. Y. To appear in *Adv. Polym. Sci.*
(4) Brown, H. R. *Macromolecules* **1991**, *24*, 2752−2756.
(5) Char, K.; Brown, H. R.; Deline, V. R. *Macromolecules* **1993**, *26*, 4164−4171.
(6) Creton, C.; Kramer, E. J.; Hui, C. Y.; Brown, H. R. *Macromolecules* **1992**, *25*, 3075−3088.
(7) Brown, H. R.; Char, K.; Deline, V. R.; Green, P. F. *Macromolecules* **1993**, *26*, 4155−4163.
(8) Boucher, E.; Folkers, J. P.; Hervet, H.; Léger, L.; Creton, C. *Macromolecules* **1996**, *29*, 774−782.
(9) Boucher, E.; Folkers, J. P.; Creton, C.; Hervet, H.; Léger, L. *Macromolecules* **1997**, *30*, 2102−2109.
(10) Plummer, C. J. G.; Kausch, H. H.; Creton, C.; Kalb, F.; Léger, L. *Macromolecules* **1998**, *31*, 6164−6176.
(11) Kanninen, M. F. *Int. J. Fracture* **1973**, *9*, 83−92.
(12) Penado, F. E. *J. Compos. Mater.* **1993**, *27*, 383−407.
(13) Van Duin, M.; Souphantong, A. *Rubber Chem. Technol.* **1995**, *68*, 717.
(14) Van Duin, M. Private communication.
(15) Kalb, F. Ph.D. Thesis, Université Paris VI, Paris, 1998.
(16) Sue, H. J. *J. Mater. Sci.* **1992**, *27*, 3098−3107.

MA001318E